Revista Mexicana de Física 31 No. 1 (1984) 25-56

INELASTIC CROSS-SECTIONS FOR FAST-ELECTRON COLLISIONS*

Rogelio Muñoz

Escuela de Físico-Matemáticas, Universidad Michoacana
Morelia, Michoacán, México

(recibido marzo 23, 1984; aceptado junio 18, 1984)

ABSTRACT

Transmission electron energy-loss has been used to determine the angular and energy dependence of the cross-section for K-shell ionization of Aℓ, and L-shell ionization of Cr, Fe, and Cu. On the basis of these experimental results it was found that simple hydrogenic theory predicts well the angular distribution of inner-shell scattering and shows a reasonable absolute agreement for a large energy window. In addition, total-inelastic cross-sections for these elements were measured and compared with the free-electron Plasmon and Hartree-Slater theory. The experiments show that a free-electron plasmon model predicts fairly well the cross-section for elements such as Aℓ. For Cr, Fe, and Cu an atomic model is more appropiate.

---

* This work is part of the thesis submitted to the Faculty of Graduate Studies and Research, University of Alberta, Canada, in partial fulfilment of the requirements for the degree of Master of Science.

RESUMEN

Usando espectroscopía de transmisión de electrones se determinó la dependencia angular y de energía de las secciones-eficaces de ionización de la capa-K en Aℓ y de la capa-L en Cr, Fe y Cu. Los resultados de estos experimentos muestran que la teoría hidrogenoide predice adecuadamente la distribución angular de los electrones que han ionizado capas internas de un átomo y muestra valores absolutos razonables para una ventana de energía grande. Además, se midieron secciones-eficaces totales de dispesión inelástica para los mismos elementos y se compararon con los valores calculados usando la teoría del electrón libre para un metal y con los valores obtenidos con la teoría Hartree-Slater. Los experimentos muestran que la teoría del plasma de electrones libres predice adecuadamente la sección-eficaz para elementos como el Aℓ. Para Cr, Fe y Cu un modelo atómico es más apropiado.

1. INTRODUCTION

With the first papers dealing with collisions of fast particles with atoms, which appeared at the beginning of this century, there began a new technique for studying the structure of the matter by means of this process. The process generally represents the interaction of particles (in this case electrons) with atoms, the latter sometimes called the target and the phenomenon itself scattering. Thus, a scattering process depends on the characteristics of the incident electrons and the atomic properties of the target (here we use the words specimen and sample as synonymous with target). The characteristics of the incident electrons depend on how fast they are approaching the scattering atom, *i.e.*, on the wavevector $\vec{k}$, while the atomic properties are generally described by probabilities of transition; these probabilities are related to the kind of atomic wave function assumed and consequently to the atomic potential. When the incident electrons interact with the atomic potential, the former may be deviated from their original direction (scattered). There are basically two types of scattering process: elastic and inelastic. In the former, the incident particles transfer momentum, and in the latter transfer momentum and appreciable energy to the atoms of the sample. This latter mechanism by which fast electrons (with kinetic energy greater than about 10keV) interact with a sample is the

main concern in the present work.

If a beam of fast electrons impinges upon a sample, and the sample is thin enough so that most of the beam is not absorbed, it is convenient to classify the transmitted electrons into three categories: (1) the unscattered beam, (2) the elastically scattered beam, and (3) the inelastically scattered beam. These groups are characterized primarily on the basis of scattering mechanism and how much energy has been lost by the electrons in passing through the material. The third group of electrons that are transmitted through a thin sample are those that have interacted with the electrons within the sample and lost energy in the process. The amount of energy lost depends largely on the material being studied. That is, the distribution of energy losses is material dependent and it is this property that we are going to use for obtaining information about the atomic properties of the sample. The utilization of the transmitted electron energy loss distribution to determine chemical and structural properties of a thin sample is known as Electron Energy-Loss Spectroscopy (EELS).

In an inelastic process, the incident electrons lose energy in the interaction with matter. This energy loss is attributable to excitation of atomic electrons, both inner-shell electrons and outer-shell electrons. The probability for any of these excitations to occur is given by the corresponding cross-section.

Cross-sections for inelastic scattering of fast electrons by atoms are of concern in many branches of Physics. One such area is electron microscopy, in particular EELS where a partial cross-section $\sigma_k(\alpha,\Delta)$ for ionization of shell k (=K, L, M, etc.) by fast incident electrons (which are thereby scattered through angle $<\alpha$ and suffer energy losses between E_k and $E_k+\Delta$, E_k being the ionization energy of shell k) is required for quantitative microanalysis of light elements[1]. Also total inelastic cross-sections σ_{in} (*i.e.*, the sum of all possible inelastic collision cross-sections) are required for estimating the local thickness of a specimen[2]. Both $\sigma_k(\alpha,\Delta)$ and σ_{in} can be measured experimentally using a thin sample of known thickness and composition or may be calculated on the basis of an atomic model. Since these calculations neglect certain

factors (such as solid state effects), it is of interest to compare the theoretical results with experimental data. In this work, we present such a comparison for Aluminum, Chromium, Iron, and Copper.

2. CALCULATIONS OF INELASTIC CROSS-SECTIONS

Inelastic cross-sections specify the probability of an incident electron being inelastically scattered by an atomic electron of a sample. The probability of an atomic electron being excited to a certain energy is given by the Generalized Oscillator Strength (GOS). The GOS is proportional to the differential cross-section, which is the main concern in this Section. Here, we are going to present the different alternatives for calculating inner-shell ionization cross-sections; and finally, we present the different methods used to calculate total-inelastic cross-sections (*i.e.*, the sum of all possible inelastic-collision cross-sections).

2.1 *General considerations*

Several mehods[3] have been developed to calculate both elastic and inelastic cross-sections, since both calculations necessarly involve the assumption of an atomic potential to calculate the atomic wave functions. These wave functions may also have an analytical form for a given atomic potential.

A mehod similar to that used to calculate elastic cross-sections can be used to calculate cross-section for inelastic collisions of fast electrons with atoms. Hence, the inelastic scattering may be treated by regarding the atom as a static center of force which gives to an electron a potential energy V(r). This potential is usually taken as spherically symmetrical. Furthermore, for sufficiently fast collisions, the influence of the incident electron upon an atom may be regarded as a suddend and weak perturbation; that is, the first Born approximation can be used. According to Born's theory[4], when a plane wave strikes the atom each volume element in the atom sends out a spherical wavelet. These wavelets start in phase but possess different amplitudes depending upon the value

of the potential at the volume element. In the first Born approximation, both the incident and scattered electrons are treated as plane waves.

The first step towards obtaining inelastic cross-sections is to calculate the probability of transition from an initial (ground) to a final (excited) state; that is, to calculate GOS (Generalized Oscillator Strength). Ideally this would be done by solving the Schrödinger equation for the complete system, *i.e.*, the wave equation which contains explicity the coordinates of both the incident and atomic electrons. The energy term is the sum of the energy of the atom in its ground state and the kinetic energy of the incident electron. The solutions of this equation are generally assumed to be separable into a function of the incident electron and another function for the atom.

The energy differential cross-section for a collision, in which and incident electron of kinetic energy T is scattered with a momentum change $\hbar\vec{K}=\hbar(\vec{k}-\vec{k}')$ and energy loss E, is given in the first Born approximation by[5,6]

$$\frac{d\sigma_n}{dE} = \int_{K_{min}}^{K_{max}} \frac{4\pi a_0}{(T/R)(E/R)} \frac{df_n(E,K)}{dE} \, d[\ell n(Ka_0)^2], \qquad (2.1)$$

where a_0 is the Bohr radius; $R=me^4/2\hbar^2=13.6eV$ is the Rydberg energy. An important point about Eq. (2.1), discovered by Bethe[5], is that the GOS, $df_n(E, K)/dE$, should be independent of T if T is sufficiently large. In such a case, the GOS can be computed from internal dynamics of the atom by means of the following relation[6]:

$$\frac{df_n(E,K)}{dE} = (E/R)(Ka_0)^2 \left| \int u_n^*(r_1,..,r_Z) \sum_{j=1}^{Z} \exp(i\vec{K}\cdot\vec{r}) u_0(r_1,..,r_Z) dr_1,...dr_Z \right|^2, \qquad (2.2)$$

with r_j being the position vector of the jth atomic electron, $u_0(r_1,..,r_Z)$ and $u_n(r_1,..,r_Z)$ the wave functions of the atomic electrons in the initial and final state. The total wave functions of the initial and final state are $\Psi_0=u_0\exp(i\vec{K}\cdot\vec{r}_j)$ and $\Psi_n=u_n\exp(i\vec{K}'\cdot\vec{r}_j)$, respectively. These, of course, should satisfy the Schrödinger equation. We may rewrite Eq. (2.2) in a

more convenient form given by

$$\frac{df_{n\ell}(E,K)}{dE} = \frac{2m_0E}{\hbar^2K^2} \sum_{\ell'} |\langle \varepsilon\ell' | \exp(i\vec{K}\cdot\vec{r}) \; | n\ell \rangle|^2 \quad , \tag{2.3}$$

where $\langle n| \; |0\rangle$ denotes an atomic matrix element between the excited state n and the ground state. This matrix element depends on the quantum numbers involved in the transition. For a single atom the possible transitions are between occupied and unoccupied single-electron states of the atom, transitions to occupied states being forbidden by the Pauli exclusion principle.

Since exact atomic wave functions for the initial and final states, $u_0 \; u_n$, are seldom available, approximate methods have been developed to calculate these wave functions. These methods have given rise to different methods for the computation of GOS by means of Eq(2.2) and consequently for the computation of inelastic cross-sections by means of Eq(2.1). Some of these methods are described in the following sections.

2.2. *Inner-shell ionization cross-sections*

By an inner-shell ionization cross-section, one means the cross-section for excitation of electrons from an inner shell of an atom to the continuum. Different approaches have been developed to carry out these calculations; some of them are based on simple hydrogenic wave functions and others are based on more sophisticated computational methods to obtain more accurate atomic wave functions. Among these methods we describe those which may be relevant to EELS.

2.2.1. The hydrogenic model

Egerton[7] has proposed the use of a simple hydrogenic model to compute partial or total K- and L-shell cross-sections needed to carry out elemental analysis be means of EELS. The model is based on previous hydrogenic approximations[5,6] which use Coulombic-type wave functions.

An important point about Coulombic-type wave functions is the choice of a screening parameter. Because the choice is crucial to all calculations involving such wave functions, we shall make some comments are about the screening parameter.

The basic assumption underlying the use of screened hydrogen-like wave functions to describe a many-electron atom is that for a single electron outside a closed shell, the field due to the nucleus and the other electrons taken together can be assumed to be spherically symmetrical, that is, to behave as $\frac{1}{r}$. Once this assumption is made, the effect of the other electrons is accomodated by replacing the nuclear charge Z by an approximate effective charge $Z_s=Z-\Delta Z$, ΔZ being a number characteristic of the n and ℓ values of the electrons in the shell. The actual choice of ΔZ would depend on what criterion one uses to compare a physical many-electron atom with its idealized hydrogenic counterpart. Having decided on this parameter, one makes another vital assumption: that for a given n and ℓ, the normalized radial wave functions for atoms of different atomic number Z are similar, *i.e.*, they are replicas of the same function on different scales (scaled wave functions).

Assumptions of the hydrogenic model.-In addition to the considerations made in Section (2.1), the hydrogenic calculations are based on the following assumptions:

(1) Relativistic effects within the atom (due to the high orbital velocity of atomic electrons, on a classical picture) are neglected. Relativistic effects due to the high velocity v_0 of the incident electron can be incorporated to first order by avoiding the approximation : $E_0=(1/2)mv^2$ instead the incident electron may be characterized be the parameter $T=(1/2)m_0v^2$, m_0=electron rest mass.

(2) In common with other calculations of inner-shell cross-sections, an atomic model is assumed. That is, solid state effects are ignored; the cross-section for a given atom (integrated over an energy range greater than 50eV) is assumed to be independent of its physical and chemi-

cal environment.

(3) Exchange effects (which are possible because the incident and atomic electrons are the same type of particle and can interchange roles) are neglected.

(4) The wave functions used for the initial and final states of 1s electrons are solutions of the Schrödinger equation for the hydrogen atom, scaled to take into account the effective potential of the nucleus.

(5) The screening effect of outer shells is accounted for (to first order) by adding to the nuclear potential energy a term E_S, corresponding to an approximately spherical distribution of outer charge. Screening of the nuclear field by the second K-electron is included by using an effective nuclear charge of $Z_S=Z-\Delta Z$, ΔZ taken as the value 0.3125 calculated by Zener[8].

(6) For L-shell ionization, the hydrogenic model in its basic form predicts too large a cross-section at an energy near the ionization edge; the calculations must be modified by adding an energy dependence to the GOS, to bring this into agreement with X-ray absorption measurements[9].

The generalized oscillator strength.- The first step towards obtaining cross-sections is to calculate the GOS for a transition which absorbs energy E and momentum $\hbar\vec{K}$ from the incident electron. In the hydrogenic model, the initial and final state, u_0 and u_n in Eq.(2.2), are scaled Coulombic wave functions which yield an analytical for the GOS which can be evaluated and integrated over scattering angle and energy loss by means of a short (<100 line) computer program[10]. The GOS, as indicated in the Section (2.1), is a fundamental property of the atom and the full momentum-transfer dependence of the ionization cross-section is implicity contained in it. The GOS for a given atom can be represented comprehensively by a 3-dimensional plot of $df_n(E,K)/dE$ as a function of $\ell n(Ka_0)^{(2)}$ and E. A surface resulting from that plot is called the Bethe surface[6]. As an example, the hydrogenic GOS for carbon K-shell excita-

tion is shown as a function of E and $\ell n(Ka_0)$ [2] in Fig.1. In this figure two main features can be observed: First, individual curves show qualitatively the angular dependence of K-shell scattering, for different amounts of energy loss. For an energy loss not much larger than the threshold value E_K, the scattering is forward-peaked (*i.e.*, is of maximum intensity at $\theta=0$) whereas for large energy loss (several times E_k) the scattered electrons are concentrated around an angle given by $(Ka_0)^2=E/R$, forming a Bethe ridge which represents hard collisions, that is, those with small impact parameter. Second, the energy dependence of GOS is represented by cross-sections through the Bethe surface at constant K: in particular, planes corresponding to very small K give the optical oscillator strength, which is poportional to the photoabsorption cross-section.

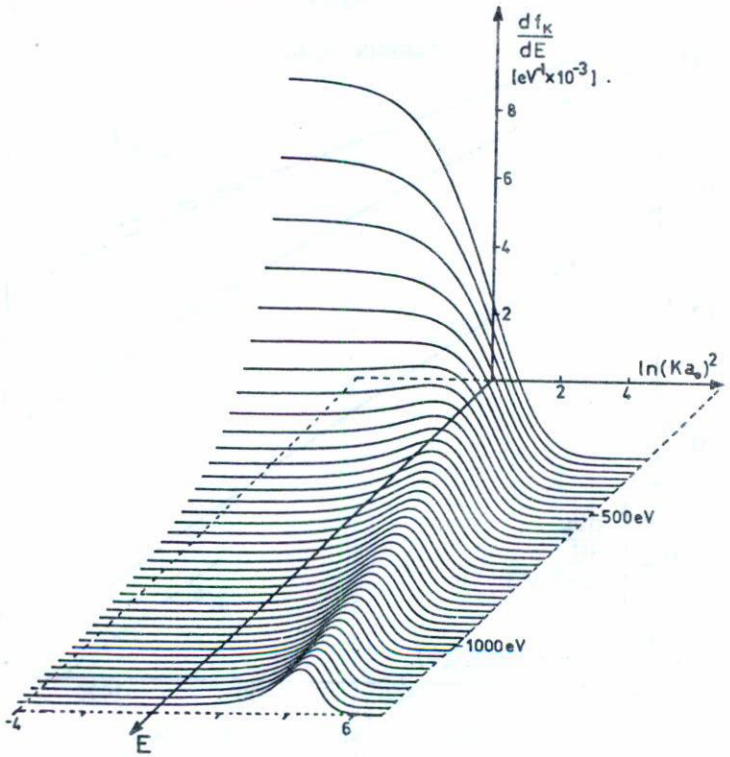

Fig. 1. The Bethe surface for K-shell ionization in carbon, calculated from the hydrogenic model [7].

The energy differential cross-section.-The number of incident electrons scattered as a result of k-shell excitation into angles less than α and energy loss E can be obtained by integration of Eq.(2.1) over appropriate limits of integration: $(Ka_0)^2_{min}$ and $(Ka_0)^2_{max}$, which may be obtained from the scattering kinematics (conservation of momentum and energy). The energy-differential cross-section, $d\sigma_k(\alpha)/dE$, computed from the hydrogenic model for various values of α and E shows (Fig. 2) an approximate energy dependence of the form

$$\frac{d\sigma_k}{dE} \propto E^{-s} \quad . \tag{2.4}$$

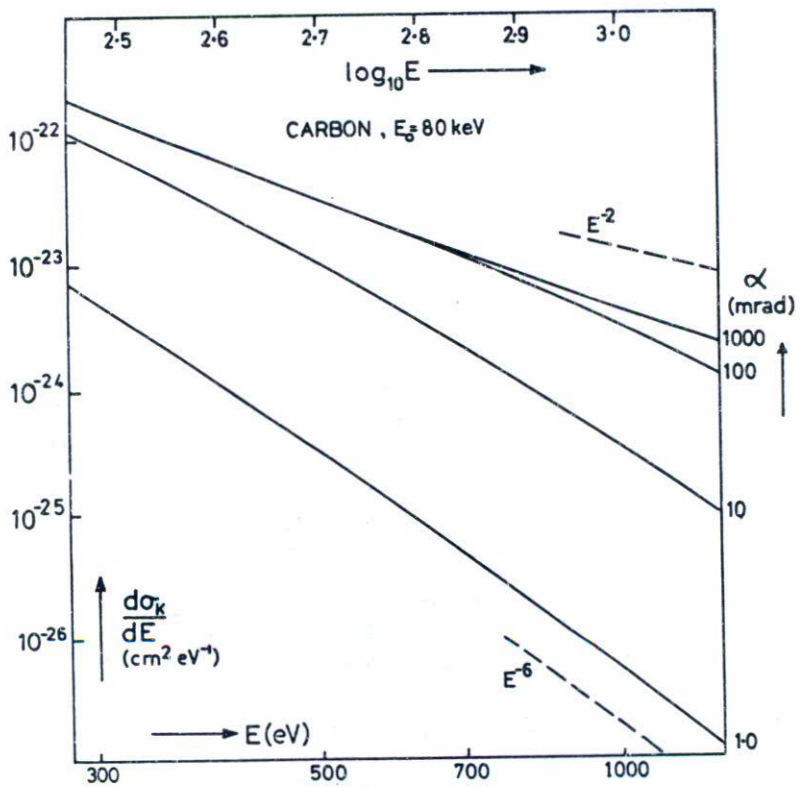

Fig. 2. The K-shell energy-loss spectrum of carbon for 80keV incident electrons and various collection semi-angle α(Ref. 7).

Partial cross-sections.- The partial cross-sections $\sigma_k(\alpha,\Delta)$, which specify the probability of k-shell scattering through angles up to α and with energy losses covering a range Δ above E_k (the binding energy), is given by

$$\sigma_k(\alpha,\Delta) = \int_{E_k}^{E_k+\Delta} \frac{d\sigma_k(\alpha)}{dE} dE. \tag{2.5}$$

For numerical integration of this equation, use was made of the approximate power-law dependence, Eq.(2.4), to reduce the number of steps required, s being calculated for each energy increment. In Section 4 we present some hydrogenic calculations for selected elements for comparison with experimental results.

Integral and total cross-sections.- For large Δ, the partial cross-section $\sigma_k(\alpha,\Delta)$ becomes equal to the integral cross-section $\sigma_k(\alpha)$ for k-shell scattering into angles up to α and energy loss above the threshold E_k. $\sigma_k(\alpha)$ can be evaluated numerically as:

$$\sigma_k(\alpha) = \int_{E_k}^{E_2} \frac{d\sigma_k(\alpha)}{dE} dE, \tag{2.6}$$

where E_2 is chosen such that contributions to the integral from higher energy losses can be neglected. In the limiting case $\alpha=\pi$, Eq(2.6) gives the total cross-section for k-shell scattering.

2.2.2 Hartree-Slater Model

A nonrelativistic Hartree-Slater central-field model was used by Leapman, Rez, and Mayers[11] to calculate cross-sections for ionization of atomic K-, L-, and M-shells by fast electrons. The *Hartree-Slater* terminology was first used by Manson[12] to indicate the use of Hartree wave functions with the Slater approximation for exchange. Manson also pointed out that the more usual *Hartree-Fock-Slater* terminology incorrectly suggests an improvement on the Fock exchange.

In the central field approximation, the radial part of the single-particle orbital satisfies the Schrö dinger equation

$$\frac{\hbar^2}{2m}\frac{d^2R}{dr^2}n\ell + \{\varepsilon - V(r) - \frac{\ell(\ell+1)\hbar^2}{2mr^2}\} R_{n\ell} = 0. \qquad (2.7)$$

Here ε is the single-particle energy eigenvalue. An interesting point about this equation is that the potential $V(r)$ seen by an electron in the orbital $(n\ell)$ depends on the orbital. To solve this equation, Hartree[13] suggested the following procedure. By associating a charge density $\rho(r)=-4\pi eR^2_{n\ell}(r)$ with each electron, we could construct a tentative potential from the total charge distribution due to the electrons and the nucleus. Solving Eq.(2.7), we could obtain solutions $R_{n\ell}(r)$ which now determine a new potential. This procedure is continued until the final wave functions is self-consistent to a high order of accurancy.

Assumptions of the Hartree-Slater Model.- The calculations carried out by Leapman, Rez, and Mayers[11] are based on previous calculation done By Manson[12] and McGuire[14] who make use of the general considerations mentioned above. In addition, the following assumptions are made.

(1) Relativistic effects within the atom are neglected. Relativistic effects due to the high velocity v of the incident electron are accounted by using $E_0=(1/2)m_0V^2$ instead of the most general expression $E=mc^2 - m_0c^2$.

(2) An atomic model is assumed. Consequently, solid state effects are neglected.

(3) Exchange between the scattered electron and the ejected atomic electron is not taken into account, since this effect is negligible except for very high energy losses and scattering angles.

(4) The initial and final states of the atom are expressed as products of one-electron wave functions for a central atomic potential. Thus, wave functions of the electrons not directly involved in the transition remain unaltered.

(5) The initial state is a one-electron Herman-Skillman wave

function, a solution of the Schrödinger equation with the self-consistent atomic potential

$$V_{1s}^{self}(r)=(2/r)\ \{1-(1+Z_0 r)\exp(-2Z_0/r)\}, \qquad (2.8)$$

where Z_0 is the effective screened nuclear charge for a 1s electron. The final states are found by solving the radial Schrödinger equation, Eq.(2.7), with the same central field for the continuum energies. The outer states are normalized by matching Coulomb wave functions at large radius.

The generalized oscillator strength.- The GOS needed to calculated the cross-sections is calculated by computing the matrix elements in the following equation (cf. Eq. 2.3):

$$\frac{df_{n\ell}(E,K)}{dE} = \frac{2m_0 E}{\hbar^2 K^2} \sum_{\ell'} |\langle \varepsilon\ell' | \exp(i\vec{K}\cdot\vec{r}) | n\ell \rangle|^2 \quad . \qquad (2.9)$$

Here, n and ℓ refer to the initial and final state principal and angular momentum quantum number, respectively, ε and ℓ' refer to the final state with continuum energy ε and angular momentum ℓ' . The energy loss E is related to ε by $E=\varepsilon-E_{n\ell}$, where $E_{n\ell}$ is the binding energy of the initial state. The computation of the matrix elements in Eq.(2.9) is carried out following Manson[12], who expanded the operator $\exp(i\vec{K}\cdot\vec{r})$ in terms of spherical Bessel functions which leave a radial integral to be evaluated numerically. The total GOS is obtained from Eq.(2.9) by summing over the final angular momentum ℓ' which is determined by the number of partial waves, that is, the number of terms in the superposition of one-electron wave functions required to describe the final state. This number was estimated as follows: the continuum wave function sees an effective potential in Eq.(2.7)

$$V_{eff} = V(r) + \frac{\ell'(\ell'+1)\hbar^2}{2m_0 r^2} \quad . \qquad (2.10)$$

For large ℓ', this is dominated by the second term, the *centrifugal poten*

tial. If the continuum energy is less than the *centrifugal potential*, overlap between the initial and continuum states is small and therefore these values of ℓ' will contribute little to the GOS. It was assumed that most of the initial state is contained within a distance a_0 (the Bohr radius), where the *centrifugal potential* is less or approximately equal to ε, that is $\{\ell'(\ell'+1)\hbar^2/2m_0a_0^2\}\lesssim\varepsilon$. For ε=1000eV, typically 10 partial waves were required to describe the continuum wave fuction. As an example of this calculations, in Fig. 3a is shown the GOS for transition into the continuum from the 2p subshell in Silicon.

The differential cross-section.- The differential cross-section, written in terms of the scattering angle, yields a double-differential cross-section which gives the energy differential cross-section per unit solid angle Ω:

$$\frac{d^2\sigma_{n\ell}(E,\theta)}{dEd\Omega} = \frac{2e^2}{m_0v^2E}\ \frac{1}{\theta^2+\theta_E^2}\ \frac{df_{n\ell}}{dE}(E,K)\ , \qquad (2.11)$$

where $\hbar^2K^2/2m_0E_0=\theta^2+\theta_E^2$ and $\theta_E=E/2E_0$. The last relation is obtained from conservation of momentum and energy in the scattering process for $E<E_0$ and $\theta<\pi$. E is the energy lost by the incident electron with energy E_0 and θ is the scattering angle.

The differential cross-section derived from the GOS by integration of Eq.(2.11) up to momentum transfer defined by different angular apertures gives rise to an energy-loss spectrum which may be used to obtain partial or total cross-sections. The energy-loss spectrum was computed within this model up to some hundreds of eV above threshold for selected elements. Some of these results are shown in Fig. 3b.

2.3 *Total-inelastic Cross-Sections*

The total cross-section for inelastic scattering σ_{in} is defined as the sum of all possible inelastic-collisions which may result from different processes. These processes are generally transitions of ground to excited states, including discrete and continuum. In this section we present two different models to calculate σ_{in}.

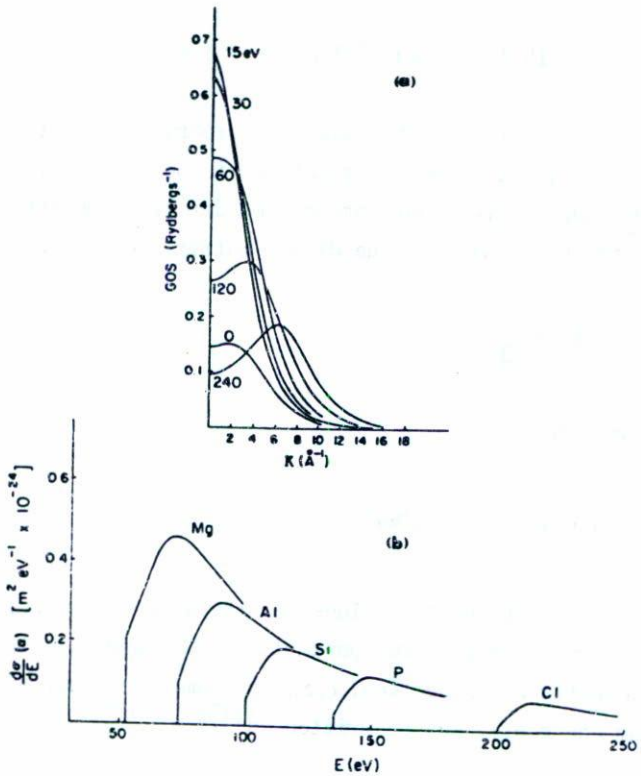

Fig. 3. (a) GOS for transition into the continuum from 2_p subshell in Silicon. (b) $L_{2\,3}$ edges for 10mrad collection angle for elements in the third period[11].

2.3.1. Total-inelastic cross-sections based on the hartree-slater model

Inokuti *et al.*[15] have reported values of two parameters involved in the evaluation of the cross-section for inelastic scattering of fast electrons by atoms. Their calculations are based on a single-electron approximation using Hartree-Slater independent-electron wave functions. In addition the first Born approximation is used.

When one integrates Eq.(2.1) over all possible values of momentum transfer $\hbar\vec{K}$ for a given excitation energy E corresponding to the state n, one obtains a compact expression called the Bethe cross-section:

$$\sigma_n = 4\pi a_0^2 (R/T)\{ M_n^2 (\ell n\{\beta^2/1-\beta^2\} - \beta^2) + C_n\}. \qquad (2.12)$$

This expressions is actually the result incorporating relativistic effects, where $\beta=v/c$, a_0, R, and T as defined in Section 2.1. The two parameters M_n^2 and C_n are atomic properties derived from the GOS. In particular, M_n^2 is the density of the dipole matrix element and is given by

$$M_n^2 = (R/E) \frac{df_n}{dE} . \qquad (2.13)$$

C_n being related to M_n^2 by

$$C_n = M_n^2 (\ell n\ c_n + 11.2268). \qquad (2.14)$$

Any sum of σ_n over different n values has the same analytical dependence on T and is characterized by two parameters M_n^2 and C_n. In particular, the total inelastic cross-section, *i.e.*, the sum of σ_n over all n (discrete and continuum energies), may be written as[15]

$$\sigma_{in} = 4\pi a_0^2 (R/T)\ \{ M_{tot}^2\ (\ell n\{\beta^2\ /1-\beta^2\} - \beta^2 + C_{tot}\}\ , \qquad (2.15)$$

where the total dipole matrix element square M_{tot}^2 is obtained by summing Eq.(2.13) over all n, that is: $M_{tot}^2 = \sum_n M_n^2$. The second quantity in the total cross-section is $C_{tot} = M_{tot}^2 \{\ell n(c_{tot}) + 11.2269\}$. According to the general theory[15] it may be evaluated by means of the relation $M_{tot}^2 \ell n(c_{tot}) = -2L(-1) + I_1 - I_2$, where L(-1) is a quantity defined by

$$L(-1) = \int (R/E)\ \ell n(E/R) \frac{df}{dE}\, dE, \qquad (2.16)$$

and the quantities I_1 and I_2 are integrals containing the incoherent scattering function $S_{in}(K)$ which is an internal state property. These quantities are given by

$$I_1 = \int_1^{\infty} ZS_{in}(K)\ (Ka_0)^{-4} d(Ka_0)^2\ , \tag{2.17}$$

$$I_2 = \int_0^{\infty} \{M_{tot}^2 - \frac{ZS_{in}(K)}{(Ka_0)^2}\}\ (Ka_0)^{-2}\ d(Ka_0)^2. \tag{2.18}$$

Thus, $\ell n(c_{tot})$ can be computed from two items of information, namely, the optical oscillator-strength distribution df/dE and the wave fuction of the initial state (most commonly the ground state).

Using the parameters, M_{tot}^2 and $M_{tot}^2\ \ell n(c_{tot})$, for different elements[15] we have evaluated Eq.(2.15) for 80keV incident electrons. The results are presented in Section 4 for comparison with the experimental results.

2.3.2 Free electron theory

It is known from the work of Bohm and Pines[16] that electrons in a solid can undergo collective or plasma oscillations of fairly defined frequency. For a free-electron plasma the frequency is given by

$$\omega_p = (n_f e^2/m\varepsilon_0)^{1/2}, \tag{2.19}$$

where n_f is the free electron density in the plasma and m and e the electron mass and charge respectively. If fast incident electrons of energy E_0 traverse a sample, they are able to excite quanta of these oscillations, known as plasmons, of energy

$$E_p = \hbar\omega_p. \tag{2.20}$$

In this scattering process the momentum and energy must be conserved. This conservation yields an equation which relates the momentum transfer $\hbar\vec{K}$ to the scattering angle θ of the incident electrons with momentum $\hbar\vec{K}$, as follows:

$$K^2 = K_{||}^2 + K_{\perp}^2 . \qquad (2.21)$$

Here $K_{\perp} = k\theta$ and $K_{||} = k\theta_E$, where $\theta_E = E_p/2E_0$ is the half-width of the angular distribution of these scattered electrons. Typical values of the plasmon energy E_p lie in the range 10-30eV.

The differential inverse mean free path for electrons which suffer a loss E_p has been calculated[17] as a function of the scattering angle θ:

$$\frac{d(1/\lambda_p)}{d\Omega} = \frac{d(n\sigma_p)}{d\Omega} = \frac{1}{2\pi a_0} \frac{\theta_E}{\theta_E^2 + \theta^2} , \qquad (2.22)$$

λ_p is the mean free path for plasmon excitation, its reciprocal value is $n\sigma_p$, n being the electron concentration per unit volume and σ_p the cross-section per atom. Integration of Eq.(2.22) gives the integral cross-section σ_p for plasmon scattering through any angle up to θ_c:

$$\sigma_p = (\theta_E/na_0) \ln(\theta_c/\theta_E). \qquad (2.23)$$

Taking calculated values of $\theta_c = k_c/k$ (k_c=critical wave vector and k=wave vector of the incident electron) for different elements an E_0=80keV, the dependence of σ_p on the atomic number Z according to Eq.(2.23) is given in Section 4 for comparison with experimental data.

3. EXPERIMENTAL DETERMINATION OF INELASTIC CROSS-SECTIONS

In the Conventional Transmission Electron Microscope (CTEM) the spectral energy distribution in the transmitted beam, which results from the interaction between the primary electron beam of energy E_0 and the specimen, contains useful information concerning the physical and chemical properties of the sample. The analysis of the energy of these transmitted electrons is in essence a kind of spectroscopy called Electron Energy-Loss Spectroscopy (EELS).

In order to carry out an energy-loss experiment to measure

inelastic cross-sections we require: (1) a source of electrons, (2) a suitable sample of the material to be studied, and (3) a device (spectrometer) for analyzing the energy of the transmitted electrons. In general, these components can take a variety of different forms, but we are mainly interested in an experimental arrangement which is compatible with the operation of a CTEM. In this case, the source of electrons will be the gun of the microscope and the incident electrons will be assumed to have a well defined energy E_0 (say 80keV). Because we are using a microscope, the incident beam will be capable of being focussed on to a specimen area whose size and position can be controlled, and which can be imaged using the normal optical system of the instrument. The specimen will be a thin film or section of the material that we wish to study; some of its characteristics will be discussed in the next Section. The spectrometer is placed after the specimen, as shown in Fig. 4, to analyze the transmitted electrons.

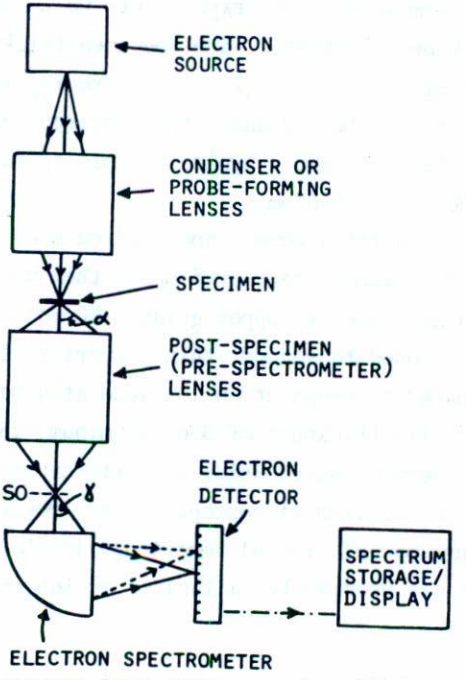

Fig. 4. Typical EELS system; lens column can be either conventional or scanning transmission microscope[24].

All the information that is obtained about the sample is contained in the angular and energy distribution of the electrons that have passed through the specimen. By studing these distribution, resulting from the interaction between the incident electrons and the sample, the required information relating to inelastic cross-sections can be measured. The method used to carry out the analysis is described below.

3.1 Sample preparation

There are many conditions which the ideal sample should fulfill (*i.e.*, have a clean surface, be homogeneous, etc.) and most preparations methods involve a compromise with respect of them. The most obvious requirement is that the specimen be transparent to electrons (with and without an objective aperture in place). In other words, that the specimen be thin enough for an electron microscope investigation.

To perform energy-loss experiments we required thin uniform films or sections of known thickness. The specimen thickness should in general satisfy the relationship[18] $t<(\lambda_{in}/2)$, where λ_{in} is the total mean free path for inelastic scattering and t the specimen thickness, which for 80keV incident electrons and a typical sample containing light elements ($Z<30$) is in the range 20-60nm.

Thin carbon films were evaporated on mica then floated off, on the surface of distilled water, by dipping them under the water and picking the up on 3-nm diameter copper grids (150 mesh per inch). These carbon films were used to support thin polycristalline metallic films which were prepared by evaporation in vacuo at a base pressure of about 10^{-5} Torr. The film thickness of 33nm Aluminum, 28nm Chromium, 24nm Iron, and 48nm Copper were measured using a quartz-crystal thickness monitor situated near the electron microscope grids. Because accurate film thickness measurements are of crucial importance in the present work the quartz-crystal monitor was previously calibrated by interferometry.*

*Experimental details are available from the author.

3.2 *Collection and analysis of an energy-loss spectrum*

To characterize the interactions of the incident electrons and the sample we collect all the transmitted electrons lying within a cone of some semi-angle α (in a CTEM this angle is limited by an objective aperture located on the back focal plane of the objective lens) about the incident beam direction, and then analyze these for their energy loss. The result that we obtain from such an experiment is an energy-loss spectrum (ELS), in which we plot the transmitted signal intensity J as a function of the energy-loss E for all the electrons scattered within the angular cone α accepted by the spectrometer. Figure 5 shows schematically an ELS. The spectrum consists of:

(1) A sharp peak at E=0 representing the elastically scattered and unscattered electrons from the incident beam (one normally refers to this as the zero-loss peak).

(2) A broad peak in the range E=10 to 40eV indicating energy loss due to excitation of plasmons or valance-electron transitions. These two peaks lie in the region of the spectrum known as the low-loss regions.

(3) An abrupt rise in the transmitted intensity representing excitation of inner shell electrons to vacant states in the continuum. This rise, in the high-loss region of the spectrum, takes place above an energy loss equal to the binding energy E_k, where k is the type of inner shell excited (k=K, 1, M, etc.).

3.2.1 Measurement of ionization partial cross-sections

The excitation edges in the ELS are normally used to identify the presence of a given element within the area of specimen defined by the incident beam of electrons. A quantitative estimation, giving the number N of atoms of the element per unit area of specimen, is obtained from the area $I_k(\alpha,\Delta)$ measured directly under an excitation edge, after extrapolating and subtracting the background wich precedes the edge (see Fig. 6). In such a case, the formalism due to Egerton[19] can ben used to

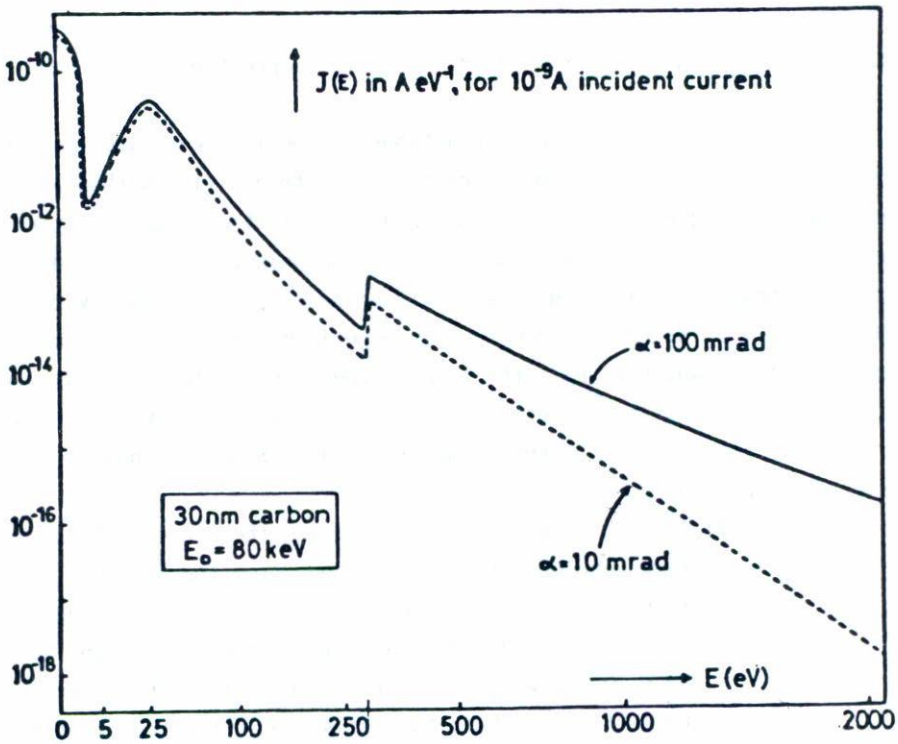

Fig. 5. Electron intensity J(E) as a function of energy loss E (the energy-loss spectrum) for 80keV electrons transmitted through a 30nm specimen of amorphous carbon. The spectrum is shown for two different values of collection semi-angle α. It exhibits (from left to right) a zero-loss peak, a valenceexcitation peak and an inner-shell edge due to excitation of 1s (K-shell) electrons. For convenience of display, non-linear scales have been used on both axes.

obtain the concentration N of a given element, *i.e.*,

$$N = \frac{1}{G} \cdot \frac{I_k(\alpha,\Delta)}{I_\ell(\alpha,\Delta)} \cdot \frac{1}{\sigma_k(\alpha,\Delta)} , \tag{3.1}$$

here $I_\ell(\alpha,\Delta)$ is an area measured from the low-loss region of the spectrum (Fig. 6) and $\sigma_k(\alpha,\Delta)$ is a partial cross-section of the element, corresponding to inner-shell losses between E_k and $E_k+\Delta$. The factor G allows for

any difference in the detector gain between the low- and the high-energy region of the spectrum.

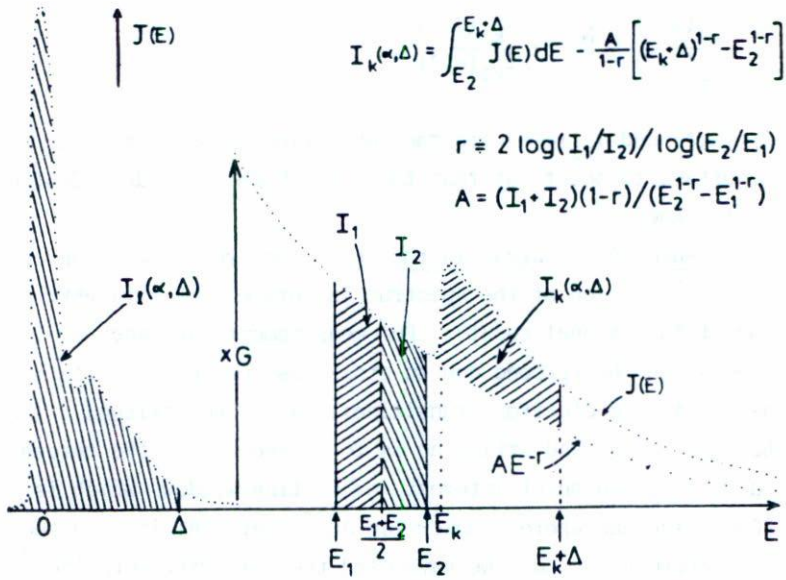

Fig. 6. Schematic energy-loss spectrum illustrating one method of background fitting and measurement of the integral $I_k(\alpha,\Delta)$ for quantitative analysis.

There are two methods, direct and indirect, in which Eq.(3.1) can be used to obtain partial ionization cross-sections. The direct method (used for elements) involves knowledge of the concentration N per unit area of specimen. This quantity is known if one takes the bulk density ρ of the element and assumes a specimen thickness t, since N is related to the concentration per unit volumen n by $N=nt=\rho N_0 t/A$, where A is the atomic weight of the constituent atoms and N_0 the Avogadro's number. Knowing N, it is possible to obtain the partial cross-sections from the same measurable quantities mentioned above (*i.e.*, $I_k(\alpha,\Delta)$ and $I_\ell(\alpha,\Delta)$). The indirect method (used for stoichiometric compounds) assumes, according to the stoichiometry, the relative abundance N_1/N_2 of the two elements in a compound. In this case the ratio of the two partial cross-sections $\sigma_{k1}(\alpha,\Delta)$ and $\sigma_{k2}(\alpha,\Delta)$ can be obtained if two excitation edges in the same spectrum

are measured under the same conditions, *i.e.*, with the same α and Δ. $I_\ell(\alpha,\Delta)$ and G in Eq.(3.1) cancel giving

$$\frac{\sigma_{k1}(\alpha,\Delta)}{\sigma_{k2}(\alpha,\Delta)} = \frac{N_1}{N_2} \cdot \frac{I_{k1}(\alpha,\Delta)}{I_{k2}(\alpha,\Delta)} , \tag{3.2}$$

where $I_{k1}(\alpha,\Delta)$ and $I_{k2}(\alpha,\Delta)$ are the quantities to be measured in the ELS It is important to point out that the ratio N_1/N_2 is independent of the specimen thickness.

Measurement of areas in the ELS.- The area $I_\ell(\alpha,\Delta)$ under the low-loss energy region of the spectrum is obtained by straightforward summation of the channel counts. For measurements on inner-shell ionization edges, the background due to other loss process (excitation of plasmons or valence-electron transitions) has to be stripped. The general method for background stripping is to define before the threshold energy E_k a fitting region of interest, or fitting window, which is typically 50 to 200eV wide and where a power law AE^{-r} (Ref. 20) is adjusted to the data. To determine A and r we have used the following formulae[21]:

$$A = (I_1+I_2)(1-r)/(E_2^{1-r} - E_1^{1-r}), \tag{3.3}$$

$$r = 2\ \log(I_1/I_2)/\log(E_2/E_1), \tag{3.4}$$

where the fitting window (E_1, E_2) is divided in two halves (Fig. 6) of respective integrals I_1 and I_2. Once the fit is made, the power law AE^{-r} is extrapolated under the characteristic edge (Fig. 6) up to few hundreds of eV. The area $I_k(\alpha,\Delta)$ is then evaluated using the relation

$$I_k(\alpha,\Delta) = \int_{E_2}^{E_k+\Delta} J(E)dE - \frac{A}{1-r}\{(E_k + \Delta)^{1-r} - E_2^{1-r}\} . \tag{3.5}$$

3.2.2 Measurement of total-inelastic cross-sections

The area I_0 under the zero-loss peak, relative to the total area I_T under the energy-loss spectrum, can be used for measuring the

total mean free path for inelastic scattering λ_{in}, according to the equation

$$\frac{t}{\lambda_{in}} = \ell n(I_T/I_0). \qquad (3.6)$$

If the thickness t is known one can find λ_{in} by measuring I_0 and I_T. These two quantities are obtained by straight forward summation of the channel counts corresponding to the zero-loss peak and to the total spectrum (typically recorded up to 2000eV for analysis of light elements). The total inelastic cross-section per atom is found using the relation $\sigma_{in}=1/n\lambda_{in}$, where n is the concentration of atoms per unit volume of specimen.

3.3 *Experimental details*

The experimental system for recording the energy loss spectrum has been described previously[22]. This consists of a JEM 100B transmission electron microscope combined with a custom-made magnetic spectrometer[23]. Using the electron microscope in the diffraction mode, a spot diameter of about 4μm at 80keV primary electrons is incident on the specimen. The transmitted electrons lying in a cone of some width α and focussed on the object plane of the spectrometer by means of an intermediate lens of the microscope operated in "high-resolution diffraction" mode (in this mode the projector lens is switched off). The electron spectrometer produces its energy dispersion by applying to the transmitted electrons a magnetic field. Spectra are recorded by scanning the exit beam of the spectrometer across an adjustable slit located at the spectrometer image plane, causing electrons of a particular energy loss to fall onto a transmission phosphor screen with a resulting voltage at the output of the photomultiplier tube.

The spectra are acquired in 1024 channels, of a TN-1710 Multichannel Analyzer (MCA), using a typical dwell time (the time for which the data is stored in each channel) of approximately 40 msec. After

acquisition the data is processed with the help of a TN-1117 Floppy disk memory system (used for recording spectra, and loading the system operating program when necessary). This is controlled by a Texas Instruments Silent 700 data terminal, which contains an alphnumeric keyboard and a silent printer. In Fig. 7 recorded spectra are shown for the different elements analyzed. The experimental inelastic cross-sections will be given in Section 4 for comparison with the theory presented in Section 2.

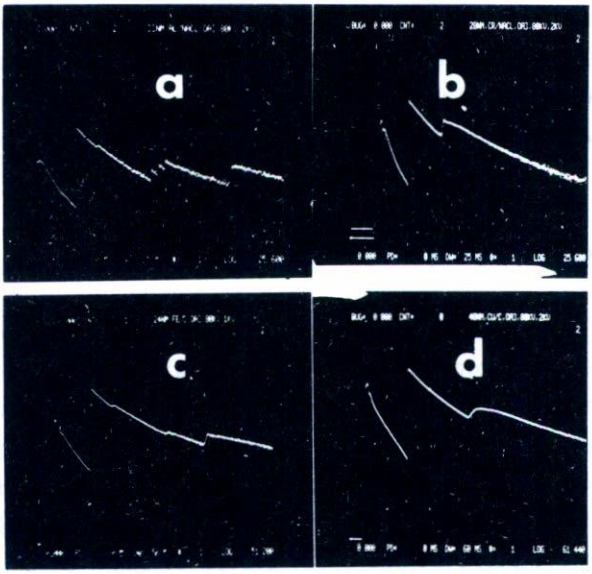

Fig. 7. Recorded spectrum from (a) a 33nm thick A_ℓ film, (b) a 28nm thick Cr film, (c) a 24nm thick Fe film, and (c) a 48nm thick Cu film.

4. COMPARISON BETWEEN CALCULATED AND EXPERIMENTAL CROSS-SECTIONS

In Section 2 the different models for calculating inelastic cross-sections were presented. In this Section we will compare the results of calculations based on these models with experimental measurements carried out for different elements (*i.e.*, Al, Cr, Fe, and Cu).

4.1 *Partial ionization cross-sections*

The cross-sections for excitation of atomic electrons from the K-shell in Al, and from the L-shell in Cr, Fe, and Cu is shown, as a function of the collection angle, in Fig. 8. In this figure, the hidrogenic calculations are compared with experimental measurements. For all the elements studied, the experimental measurements show, within the experimental standard deviation, a similar trend as the hydrogenic calculations. This similarity indicates that the hydrogenic model predicts well the angular distribution of the scattered electrons which have excited inner-shell atomic electrons. A similar comparison with the Hartree-Slater calculations is not possible, due to the lack of published data. However, the angular distribution predicted by the Hartree-Slater model can be obtained from Eq.(2.11); this equation shows that $d^2\theta/dEd\Omega$ is proportional to $1/\theta^2 + \theta_E^2$. By integrating $d^2\sigma/dEd\Omega$ over a unit of solid angle $d\Omega$, it can be seen that $d\sigma(\alpha)/dE$ is proportional to $\ell n\{1+(\alpha/\theta_E)^2\}$. In fact, this results from small angle approximation which can be justified because we are in the dipole region (momentum transfer $\hbar\vec{K}=0$). In Fig. 8b we compare a single calculation based on this model with the experiment. Agreement is closer than with hydrogenic value, which may be a result of the more accurate wave functions used for calculating the GOS.

Figure 8 shows the partial ionization cross-sections (for K-shell excitation in Al, L-shell excitation in Cr, Fe, and Cu) integrated up to two different energy windows Δ=100eV and Δ=200eV. In this figure we compare the hydrogenic calculations with experimental data. On the one hand, the experimental values do not lie consistently below or above the values predicted by the hydrogenic calculations (of. figures). This inconsistency can be attributed to the fact that the hydrogenic model does not predict well the shape of the edge near the threshold. For example the L-edge for Cr shows a slight peak at the threshold (see Fig. 7b) which is presumably due to excitation of electrons from the 2p-subshell to the partially filled 2d-subshell. This peak at the threshold contributes to the partial ionization cross-section, so we expect the experimental measurements to lie above the hydrogenic calculations, as observed in figure 8b. For the other elements studied (*i.e.*, Al, Fe, and Cu) the edges are

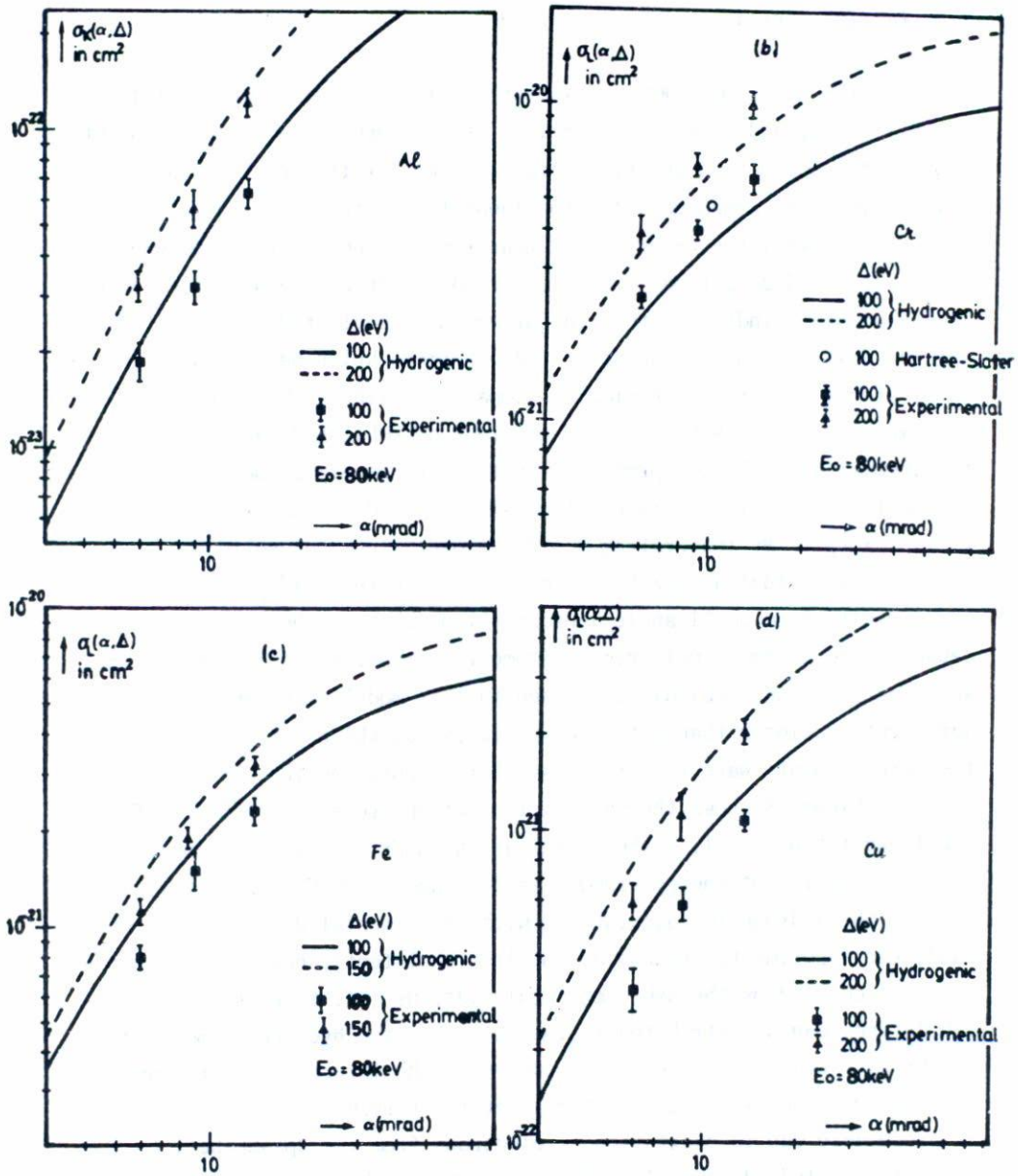

Fig. 8. Calculated and experimental cross-sections for excitation of atomic electrons from the k-shell of Aℓ, and from the L-shell of Cr, Fe, and Cu.

not peaked at the threshold and the experimental values lie below the hydrogenic calculations. That is, the hydrogenic model predicts slightly high values for the cross-section. On the other hand, when the partial ionization cross-sections for L-shell excitation (both experimental and hydrogenic) are integrated up to an energy wuindow Δ=200eV, the agreement between the experiment and theory becomes better (see Fig. 8). The disagreement for small energy window (Δ<200eV) might be expected; since the hydrogenic model in its basic form predicts too large a cross-section near the edge, the program used for calculating the cross-section for L-shell excitation adds an extra energy dependence to the GOS, to bring this in to agreement with X-ray absorption measurements[9]. If this modification is not exact, the percentage error is less for large energy window. For the elements studied the hydrogenic model agrees, within the experimental standard deviation, with the experiment for an energy window Δ=200eV.

It is relevant to point out that the error bars shown along with the experimental values represent the experimental standard deviation calculated from 10 separate measurements on each element studied. In addition, it is important to discuss possible sources of systematic error which could effect our results. First, there may be a systematic error arising from the thickness measurement. This error is estimated to be about 5%. Secondly, error may arise both from the instrument itself and from the experimental procedure. In extreme cases, this procedural error may be as high as 20% (Ref. 19).

4.2 Total-inelastic cross-sections

In Fig. 9 the cross-sections for inelastic scattering, based on the Plasmon and Hartree-Slater models, are shown as a function of the atomic number (Z), for comparison with the experimental measurements. The experimental values for Cr, Fe, and Cu are all greater than predicted by Plasmon calculations, whereas for Al this model gives the best agreement. This good agreement is no doubt because Al is more like a free-electron metal than the other metals, as can be seen from the fact that the experimental plasmon energy (16eV) is approximately equal to that predicted by

the free-electron plasmon theory (15.8eV). For the other elements the energy difference is appreciable (*e.g.*, for Cr 18.5 and 27eV, for Fe 16.7 and 23eV respectively) so we might expect the cross-section to be given more accurately be the Hartree-Slater model, as in fact is observed in Fig. 9. For all, the experimental value is a factor of 2.6 less than predicted by Hartree-Slater calculations. This large discrepancy is probabily due to solid-state effects, which shift the oscillator strength to higher energy loss. This shift can be seen from the fact that in a single Al atom the ionization energy is 5.99eV, whereas in the solid the plasmon energy is approximately 16eV. The energy shift decreases the cross-section, since $d\sigma/dE$ is proportional to$(1/E)df/dE$ {cf. Eq.(2.1)}.

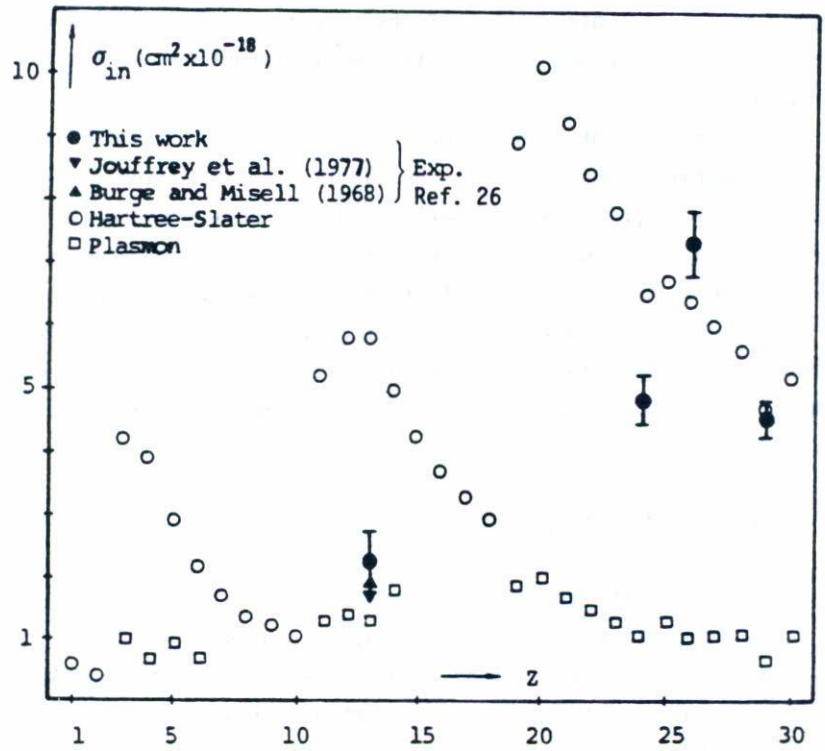

Fig. 9 Inelastic cross-section as a function of the atomic number (Z) for 80keV electrons. The calculations are based on the Hartree-Slater and Plasmon model.

5. CONCLUSIONS

Comparison between the hydrogenic model and experiment indicates that for all the elements studied the former predicts well the angular distribution of the scattered electrons which have excited inner-shell atomic electrons. Although these measurements were carried out only for a few elements we might expect similar results for other elements. The comparison also indicates that the hydrogenic model is less accurate for calculating L-shell cross-sections with low energy windows (Δ<200eV). This discrepance between theory and experiment may be due to both atomic and solid-state fine structure near the edge. On basis of the present experimental results this effect was found to be less for a large energy window (Δ=200eV).

Comparison between the different models for calculating total-inelastic cross-sections and experiment indicates that no single model predicts well the cross-section. However, the cross-section for metals whose valence losses are mainly due to single-electron transitions should be predicted more accurately be atomic models. Furthermore, for metals (like Al) whose valence losses are mainly due to collective excitations, the cross-section should be predicted more accurately by the plasmon free-electron theory.

For estimating the local thickness t of a specimen, by means of Eq.(3.6), it would be convenient to have a model for calculating the required mean free path for inelastic scattering. On the basis of the present experimental results the mean free path for free-electron metals (*e.g.* Mg, Ca, In, Sn, Cs, and Rb) can, in principle, be estimated using the plasmon free-electron theory. For elements like Cr, Fe, and Cu the mean free path can be estimated using the Hartree-Slater model. However, in many cases (*e.g.*, compounds and organic substances) it is not obvious which model is more appropriate. In this case one must rely on experimental measurements of the inelastic mean free path.

ACKNOWLEDGEMENTS

I would like to thank Professor R.F. Egerton for directing this work and making the laboratory facilities at The University of Alberta, Canada, available to me. I would also like to thank the Consejo Nacional de Ciencia y Tecnología (CONACYT) for a scholarship.

REFERENCES

1. D.C. Joy, R.F. Egerton, and D.M. Maher, *Scanning Electron Microscopy*, Ed. Ojohari, Chicago: SEM Inc. (1979) p. 817.
2. J. Hosoi, T. Oikawa, M. Inoue, Y. Kokubo, and K. Hama, *Ultramicroscopy* 7 (1981) 147.
3. D.R. Hartree, *The calculations of atomic structures*, John Wiley and Sons Inc., New York (1957); E. Fermi, Z. *Physick*, 48 (1928) 73; R.A. Fock, *Phys. Rev.*, 61 (1930) 126; J.C. Slater, *Phys. Rev.*, 35 (1930) 210; L.H. Thomas, *Proc. Cambridge Phil. Soc.*, 23 (1926) 542.
4. M. Born, Z. *Physik*, 37 (1926) 863.
5. H. Bethe, *Annal. Phys.*, 5 (1930) 325.
6. M. Inokuti, *Rev. Mod. Phys.*, 43 (1971) 297.
7. R.F. Egerton, *Ultramicroscopy*, 4 (1979) 169.
8. C. Zener, *Phys. Rev.*, 36 (1930) 51.
9. R.F. Egerton, *Proc. EMSA*, (1981) 198.
10. A FORTRAN listing of the "SIGMAK" and "SIGMAL" programs are avilable from the author (Ref. 7) on request.
11. R.D. Leapman, P. Rez, and D.F. Mayers, *J. Chem. Phys.*, 72 (1980) 1932.
12. S.T. Manson, *Phys. Rev.*, A6 (1972) 1013.
13. D.R. Hartree, *Proc. Cambridge Phil. Soc.*, 24 (1928).
14. E.J. McGuire, *Phys. Rev.*, A3 (1971) 267.
15. M. Inokuti, R.P. Saxon, and J.L. Dehmer, *Int. J. Radiat, Phys. Chem.*, 7 (1975) 109; M. Inokuti, J.L. Dehmer, T. Bear, and J.D. Hanson, *Phys. Rev.*, 23 (1981) 95.
16. D. Bohm and D. Pines, *Phys. Rev.*, 92 (1953) 609.
17. R.A. Ferrel, *Phys. Rev.*, 101 (1956) 554.
18. N.J. Zaluzec, *Proc. EMSA*, (1980) 112.
19. R.F. Egerton, *Ultramicroscopy*, 3 (1978) 243.
20. R.F. Egerton, *Philos. Mag.*, 31 (1975) 199.
21. R.F. Egerton, *Proc. EMSA*, (1980) 130.
22. R.F. Egerton, *Ultramicroscopy*, 4 (1979) 221
23. R.F. Egerton, *Ultramicroscopy*, 3 (1978) 39.
24. R.F. Egerton, *Microbeam Analysis* (Ed. K.F.J. Heinrich), (1982) 43.
25. R.E. Burge and D.L. Misell, *Philos. Mag.*, 18 (1968) 216; B. Jouffrey, Y. Kihn, J.Ph Perez, J. Sevely, and G. Zanchi, *Fifth International Conference on High Voltage Electron Microscopy, Kyoto, Japan.* (1977).